Progress in Fractional Differentiation and Applications
An International Journal

http://dx.doi.org/10.18576/pfda/110103

Certain Traveling Wave Solutions for Fractional Extended Nonlinear Schrödinger Equations

Rania Momani[1], *Asad Frihat*[2], *Mohammed Alabedalhadi*[2,*] *and Shrideh Al-Omari*[1]

[1] Department of Mathematics, Faculty of Science, Al-Balqa Applied University, Salt 11134, Jordan
[2] Department of Applied Science, Ajloun College, Al-Balqa Applied University, Ajloun 26816, Jordan

Received: 2 Dec. 2023, Revised: 18 Mar. 2024, Accepted: 13 Apr. 2024
Published online: 1 Jan. 2025

Abstract: The fractional extended nonlinear Schrödinger equation is investigated in this study. We effectively convert the governing model into a nonlinear ordinary differential equation using a sophisticated traveling wave transformation. By employing the Ansatz approach, we generate and study traveling wave solutions, specifically bright and kink wave solutions that satisfy certain parameter requirements. To gain deeper insights into the physical properties of the resulting traveling wave solutions, we employ 3D and 2D graphs at specific parameter values. This visualization provides valuable information about the characteristics and behavior of the solutions. Furthermore, we explore the influence of the fractional derivative on the obtained solution characteristics. Our research findings contribute to the understanding of nonlinear dynamics and demonstrate the existence and characteristics of bright and kink wave solutions in the fractional extended nonlinear Schrödinger equation. Moreover, we enhance our understanding of fractional derivatives and their effects on wave propagation in nonlinear media.

Keywords: Schrödinger equation; fractional derivative; traveling wave solutions; bright wave solutions; kink wave solutions.

1 Introduction

A fundamental equation that appears in many areas of physics, including condensed matter physics, plasma physics, and nonlinear optics, is the nonlinear Schrödinger equation (NLSE). Its capacity to explain a variety of nonlinear wave phenomena and soliton dynamics has led to substantial study. The NLSE is a complex partial differential equation (PDE) that takes into consideration how nonlinearity and dispersion interact. It controls how an envelope of a wave packet that is traveling in a nonlinear medium change over time. Since the NLSE considers both linear and nonlinear effects, it makes it possible to study complex wave dynamics, such as soliton generation, self-focusing, and wave propagation in nonlinear media [1-5]. Researchers have expanded the NLSE to accommodate more realistic settings and new effects. The extended nonlinear Schrödinger equation is the result of this. Numerous aspects, including higher-order dispersion, higher-order nonlinearity, and external perturbations, are frequently considered in these expansions [1,2]. Wave propagation in intricate physical systems is more thoroughly and precisely described by the extended nonlinear Schrödinger equation (NLSE). By accounting for additional effects and disturbances, the extended NLSE allows a better understanding of phenomena that cannot be fully captured by the basic NLSE. Researchers can investigate and characterize unique wave dynamics, such as rogue waves, nonlocal interactions, and the impact of external fields, using the extended version of the equation [6,7].

Understanding the behavior and characteristics of quantum systems, as represented by equations like the Schrödinger equation, depends critically on traveling wave solutions [8,9]. These insights into the dynamics of quantum processes enable us to investigate and explain the behavior of quantum particles and wave packets. The Schrödinger equation is a fundamental concept in quantum physics, illustrating how quantum states evolve over time. It is a partial differential equation (PDE) that takes into account the wave-like behavior of particles and provides a method for calculating the probabilities of various outcomes in quantum systems [10,11]. The wave function, which describes the quantum state and encodes data about the particle's position, momentum, and energy, can be found by solving the Schrödinger equation. Existence of traveling wave solutions is one of the fundamental ideas in the study of the Schrödinger equation and other quantum physics equations [12,13]. These solutions depict wave packets that maintain their shape and properties as they

* Corresponding author e-mail: mohmdnh@bau.edu.jo

move through space and time. It is possible to think of them as confined particles or quasi-particles with clearly defined characteristics like energy, momentum, and position [14,15]. Quantum physics traveling wave solutions offer several significant benefits and discoveries. First of all, they give us the ability to examine how quantum systems behave in diverse situations and potential fields. We can comprehend quantum physics concepts like interference, diffraction, and scattering by looking at how wave packets move across space and time. We are able to predict the behavior of quantum particles and the results of measurements thanks to these solutions. The genesis and behavior of quantum phenomena like solitons can also be understood using traveling wave solutions. Solitons are self-reinforcing wave packets that keep their form and speed while they travel through space. They can occur in nonlinear quantum systems and have significant effects on fields including field theory, nonlinear optics, and condensed matter physics [16,17]. Solitons' dynamics and physical characteristics can be studied to learn more about the stability and nonlinearity of quantum systems. In quantum systems, it is also possible to observe the quantization of energy and momentum through traveling wave solutions [**?**,**?**,**?**]. By imposing boundary conditions and limits on the wave functions, discrete energy levels can be generated and the quantized nature of physical observables can be established [**?**]. Consequently, energy states become quantized and discrete spectra are predicted, both of which have been empirically verified in various quantum systems. The goal of this paper is to investigate the fractional extended nonlinear Schrödinger equation (FENSE) as follows [**?**]:

$$i\left({}_i\mathscr{D}_{M,x}^{\eta,\,\alpha}\phi + a_1\mathscr{D}_{M,t}^{\eta,\,\alpha}\phi\right) - \frac{a_2}{2}\mathscr{D}_{M,t}^{\eta,\,\alpha}\mathscr{D}_{M,t}^{\eta,\,\alpha}\phi + \mu|\phi|^2\phi + ib_1\mathscr{D}_{M,t}^{\eta,\,\alpha}\left(|\phi|^2\phi\right) + ib_2\phi\mathscr{D}_{M,t}^{\eta,\,\alpha}(|\phi|^2) - i\frac{a_3}{6}\mathscr{D}_{M,t}^{\eta,\,\alpha}\mathscr{D}_{M,t}^{\eta,\,\alpha}\mathscr{D}_{M,t}^{\eta,\,\alpha}\phi = 0, \tag{1}$$

where $\phi \equiv \phi(t,x)$ is the envelope of the electric field and $\mathscr{D}_M^{\eta,\,\alpha}$ is the truncated M-fractional derivative of order α. The parameters a_1, a_2 and a_3 represents the inverse of the group velocity, the second and third order dispersion parameters, respectively. The parameter b_1 is the coefficient of the derivative cubic term, while b_2 symbolize the soliton self-frequency shift. Finally, μ represents the effective nonlinear coefficient.

We intend to develop traveling wave solutions for the FENSE (1) using a complex traveling wave transformation and the Ansatz approach. The creation of bright and kink wave solutions, which are significant wave occurrences in nonlinear systems, will be the subject of our particular attention. Under specific parameter conditions, we will examine the characteristics and behaviors of these solutions. This study was inspired by an interest in investigating the consequences of the fractional extension of the NLSE in wave propagation processes. For the analysis of complex nonlinear systems, the fractional calculus technique offers a potent mathematical tool for capturing memory and long-range interactions. The investigation of the fractional extended NLSE and the suggested methods are what make this study new. The research successfully applies a complex traveling wave transformation to transform the governing model into a nonlinear ordinary differential equation (ODE). This transformation makes it possible to analyze the system more easily and makes it easier to look at traveling wave solutions.

The paper organized to be introduction as first section. A brief review for the truncated M-fractional derivative and its properties introduced in Section 2. We utilized a suggested traveling wave transformation that reduced the model (1) into nonlinear ODE in Section 3. Section 4 devoted to obtaining the desired wave solutions using the Ansatz method. Some conclusions and discussions have presented in the last section.

2 Preliminaries

Since the advent of the concept of fractional calculus, there are several definitions for fractional operators, differential or integral, have been introduced in the literature, in particular, Riemann-Liouville [22], Caputo [23], Hadamard [24], Caputo-Hadamard [25], Riesz [26], conformable [27], local M-derivative and others [28-29]. With the existence of these various definitions, we wonder about the gauges that these operators must achieve, whether differential or integrative, so that we can call them fractional operators. Machado and Ortigueira [30] debated the concepts implicit for those definitions and indicated common attributes that should be achieved by those operators to be consider fractional. Katugampola, in turn, criticized the criteria discussed because there were operators that one could consider fractional even though they did not meet those criteria [31]. In this work, we consider the derivative in a truncated M-fractional sense. In 2018, Sousa and Oliveira introduced a truncated M-fractional derivative definition involving a truncated Mittag-Leffler function with one parameter [32,33]. This definition has unified four extant fractional derivatives from the above mentioned, as well as it satisfies some classical properties like linearity, composition, chain rule and others. In this section, we present the definition of the truncated M-fractional derivative and its essential properties that will be utilized to gain our goal in this work. Firstly, we present the definition of the truncated Mittag-Leffer function.

Definition 1 [33]. The truncated Mittag-Leffer function having one parameter is stated as

$$E_\eta^i(z) = \sum_{n=0}^{i} \frac{z^n}{\Gamma(\eta n+1)}, \tag{2}$$

where $\eta > 0$ and $z \in \mathbb{C}$.

Definition 2 [33]. Let $u : [0, \infty) \to \mathbb{R}$. Then, the truncated M-fractional derivative of the function u of order α is acquainted as follows:

$$ {}_i\mathscr{D}_M^{\eta,\,\alpha}(u(\zeta)) = \lim_{\varepsilon \to 0} \frac{u\left(\zeta E_\eta^i\left(\varepsilon \zeta^{1-\eta}\right)\right) - u(\zeta)}{\varepsilon}, \ \forall \zeta > 0 \tag{3} $$

where $0 < \alpha < 1$ and $\eta > 0$. If the truncated M-fractional derivative of the function u of order α exists, then the function u is said to be α-differentiable.

Theorem 1 [33]. Let $0 < \alpha \leq 1, \eta > 0, \ a, \ b \in \mathbb{R}$ and let the functions u and v be α-differentiable at a point $\zeta > 0$. Then, the following are satisfied:

1. ${}_i\mathscr{D}_M^{\eta,\,\alpha}(au + bv)(\zeta) = a\,{}_i\mathscr{D}_M^{\eta,\,\alpha}(u(\zeta)) + b\,{}_i\mathscr{D}_M^{\eta,\,\alpha}(v(\zeta))$.
2. ${}_i\mathscr{D}_M^{\eta,\,\alpha}(u.v)(\zeta) = u(\zeta)\,{}_i\mathscr{D}_M^{\eta,\,\alpha}(v(\zeta)) + v(\zeta)\,{}_i\mathscr{D}_M^{\eta,\,\alpha}(u(\zeta))$.
3. ${}_i\mathscr{D}_M^{\eta,\,\alpha}\left(\frac{u}{v}\right)(\zeta) = \frac{v(\zeta)\,{}_i\mathscr{D}_M^{\eta,\,\alpha}(u(\zeta)) - u(\zeta)\,{}_i\mathscr{D}_M^{\eta,\,\alpha}(u(\zeta))}{(v(\zeta))^2}$.
4. ${}_i\mathscr{D}_M^{\eta,\,\alpha}(c) = 0$, where $u(\zeta) = c$ is a constant.
5. If the function u is differentiable, then we have: ${}_i\mathscr{D}_M^{\eta,\,\alpha}(u(\zeta)) = \frac{\zeta^{1-\alpha}}{\Gamma(\eta+1)}\frac{du(\zeta)}{d\zeta}$.

The properties in Theorem 1 play an important role in this work as they will be pivotal, with the aid of a suitable traveling wave transformation, in reducing the governing model (1) into integer-order ordinary differential equation, from which the desired traveling wave solutions can be derived [34-36].

3 Traveling wave transformation

In this section, we utilize a suitable complex traveling wave transformation to reduce the governing model into a nonlinear integer-order ODE. Consider the following complex traveling wave transformation:

$$ \phi(t,x) = \Phi(\chi) \times Exp\left[i\Sigma(x,t)\right], \tag{4} $$

where $\Phi(\chi)$ gives the structure of the wave profile, $\chi = \frac{\Gamma(\eta+1)}{\alpha}x^\alpha - v\frac{\Gamma(\eta+1)}{\alpha}t^\alpha$ while $\Sigma(x,t) = \rho\frac{\Gamma(\eta+1)}{\alpha}x^\alpha + \sigma\frac{\Gamma(\eta+1)}{\alpha}t^\alpha + \delta$ symbolize the phase factor of the soliton. The parameters, ρ, σ, δ and v refers to the wave frequency, wave number, phase constant, and velocity of the wave, respectively. Using the proposed transformation with the aid of the properties of the truncated M-fractional derivative reduces the governing model into complex nonlinear -integer-order ODE, its real part obtained as:

$$ \left(\frac{a_3\sigma v - a_2 v^2}{2}\right)\frac{d^2\Phi}{d\chi^2} + (\mu - \sigma)\Phi^3 + \left(\frac{a_2\sigma^2}{2} - \frac{a_3\sigma^3}{6} - a_1\sigma - \rho\right)\Phi = 0, \tag{5} $$

while the imaginary part is given as:

$$ \frac{a_3 v^3}{6}\frac{d^3\Phi}{d\chi^3} - v\left(3b_1 + 2b_2\right)\Phi^2\frac{d\Phi}{d\chi} + \left(1 - a_1 v - \frac{a_3\sigma^2 v}{2} + a_2\sigma v\right)\frac{d\Phi}{d\chi} = 0. \tag{6} $$

Integrate (6) with respect to χ, we get:

$$ \frac{a_3 v^3}{6}\frac{d^2\Phi}{d\chi^2} - \frac{v}{3}\left(3b_1 + 2b_2\right)\Phi^3 + \left(1 - a_1 v - \frac{a_3\sigma^2 v}{2} + a_2\sigma v\right)\Phi = 0. \tag{7} $$

Applying the homogeneous balance between (5) and (7), we obtain the following results for the effective nonlinear coefficient μ and the wave frequency ρ, respectively:

$$ \mu = \frac{v\sigma a_3 + 3v a_2 b_1 - 3\sigma a_3 b_1 + 2v a_2 b_2 - 2\sigma a_3 b_2}{v a_3}, \tag{8} $$

$$ \rho = -\frac{-18v^2\sigma a_2^2 + \sigma a_3\left(18 + 6(-3+v)v a_1 + (-9+v)v\sigma^2 a_3\right) + 6v a_2\left(-3 + 3v a_1 + (3+v)\sigma^2 a_3\right)}{6v^2 a_3}. \tag{9} $$

We will use the nonlinear ODE (7) to establish traveling wave solutions for the FENSE (1).

4 Traveling wave solutions

In this section, we try to construct traveling wave solutions for the governing model (1). We seek to obtain bright wave solutions using two formulas. In addition, we will establish kink wave solutions. Both types of the desired solutions will be obtained by utilizing the Ansatz method, which approach assumes the solution of the ODE (7) can be written in specific formulas involving hyperbolic functions. Then these assumed expressions for the solution will be substituted in the ODE (7) to get an algebraic system, in which its solutions determined the undetermined parameters.

4.1. Bright wave solution I

To obtain bright wave solutions for the FENSE (1), we assume that the nonlinear ODE (7) has a solution in the form:

$$\Phi(\chi) = \Pi_1 sech(\Pi_2 \chi), \tag{10}$$

where Π_1 and Π_2 are constants to be determined. Substitute (10) into the ODE (7) and collect the coefficients of the linearly independent terms, we get an algebraic system has the following solutions:

Case 1:

$$b_1 = -\frac{2b_2}{3}, \sigma = \frac{\nu a_2 + \sqrt{\nu^2 a_2^2 + 2\nu a_3 - 2\nu^2 a_1 a_3}}{\nu a_3}, \ \nu a_3 \neq 0, \tag{11}$$

Case 2:

$$b_1 = -\frac{2b_2}{3}, \sigma = \frac{\nu a_2 - \sqrt{\nu^2 a_2^2 + 2\nu a_3 - 2\nu^2 a_1 a_3}}{\nu a_3}, \ \nu a_3 \neq 0, \tag{12}$$

where Π_1 and Π_2 are arbitrary constants. Using the obtained results (11) and (12) into (8) and (9), we obtain the following results for the effective nonlinear coefficient μ and the wave frequency ρ, respectively:

$$\mu_{1,2} = \frac{\nu a_2 \pm \sqrt{\nu^2 a_2^2 + 2\nu a_3 - 2\nu^2 a_1 a_3}}{\nu a_3}, \tag{13}$$

$$\rho_{1,2} = \frac{\nu^2 a_2^3 - 3\nu^2 a_1 a_2 a_3 \pm \left(\nu a_2^2 - (1 + 2\nu a_1) a_3\right) \sqrt{\nu^2 a_2^2 + 2\nu a_3 - 2\nu^2 a_1 a_3}}{3\nu^2 a_3^2}. \tag{14}$$

Consequently, with the aid of the complex traveling wave transformation (4), we get the following bright wave solutions for the FENSE (1):

$$\begin{aligned} \phi_1(t,x) = {} & \Pi_1 sech\left(\Pi_2\left(\frac{\Gamma(\eta+1)}{\alpha}x^\alpha - \nu\frac{\Gamma(\eta+1)}{\alpha}t^\alpha\right)\right) \\ & \times Exp\left[i\left(\rho_1\frac{\Gamma(\eta+1)}{\alpha}x^\alpha + \left(\frac{\nu a_2 + \sqrt{\nu^2 a_2^2 + 2\nu a_3 - 2\nu^2 a_1 a_3}}{\nu a_3}\right)\frac{\Gamma(\eta+1)}{\alpha}t^\alpha + \delta\right)\right], \end{aligned} \tag{15}$$

$$\begin{aligned} \phi_2(t,x) = {} & \Pi_1 sech\left(\Pi_2\left(\frac{\Gamma(\eta+1)}{\alpha}x^\alpha - \nu\frac{\Gamma(\eta+1)}{\alpha}t^\alpha\right)\right) \\ & \times Exp\left[i\left(\rho_2\frac{\Gamma(\eta+1)}{\alpha}x^\alpha + \left(\frac{\nu a_2 - \sqrt{\nu^2 a_2^2 + 2\nu a_3 - 2\nu^2 a_1 a_3}}{\nu a_3}\right)\frac{\Gamma(\eta+1)}{\alpha}t^\alpha + \delta\right)\right]. \end{aligned} \tag{16}$$

Gordon demonstrates that the term b_2 is equivalent to the retarded Raman effect [**?**], whereby the higher-frequency soliton spectrum components transfer energy to the lower-frequency components. As a result, this term causes a nonlinear dissipation, which, as seen in [**?**], causes a downshift in the soliton's carrier frequency. The existence of this phenomenon was not taken into consideration in prior hypotheses [**?**]. We depicted the obtained results in Figures 1–3, considering special values for the parameters $\Pi_1 = \Pi_2 = 1$, the group velocity, and the second and third-order dispersion parameters $a_1 = 0.008$, $a_2 = 0.005$, $a_3 = 0.025$, respectively, phase constant $\delta = 1$ and Mittag-Leffer function parameter $\eta = 1$. In Figure 1, we show the bright wave solution $\phi_1(t,x)$ for the FENSE (1) in 3D and 2D plots where the fractional derivative α considered in two cases: $\alpha = 1$ and $\alpha = 0.95$. This is important to show the variety in the the behavior of the inferred

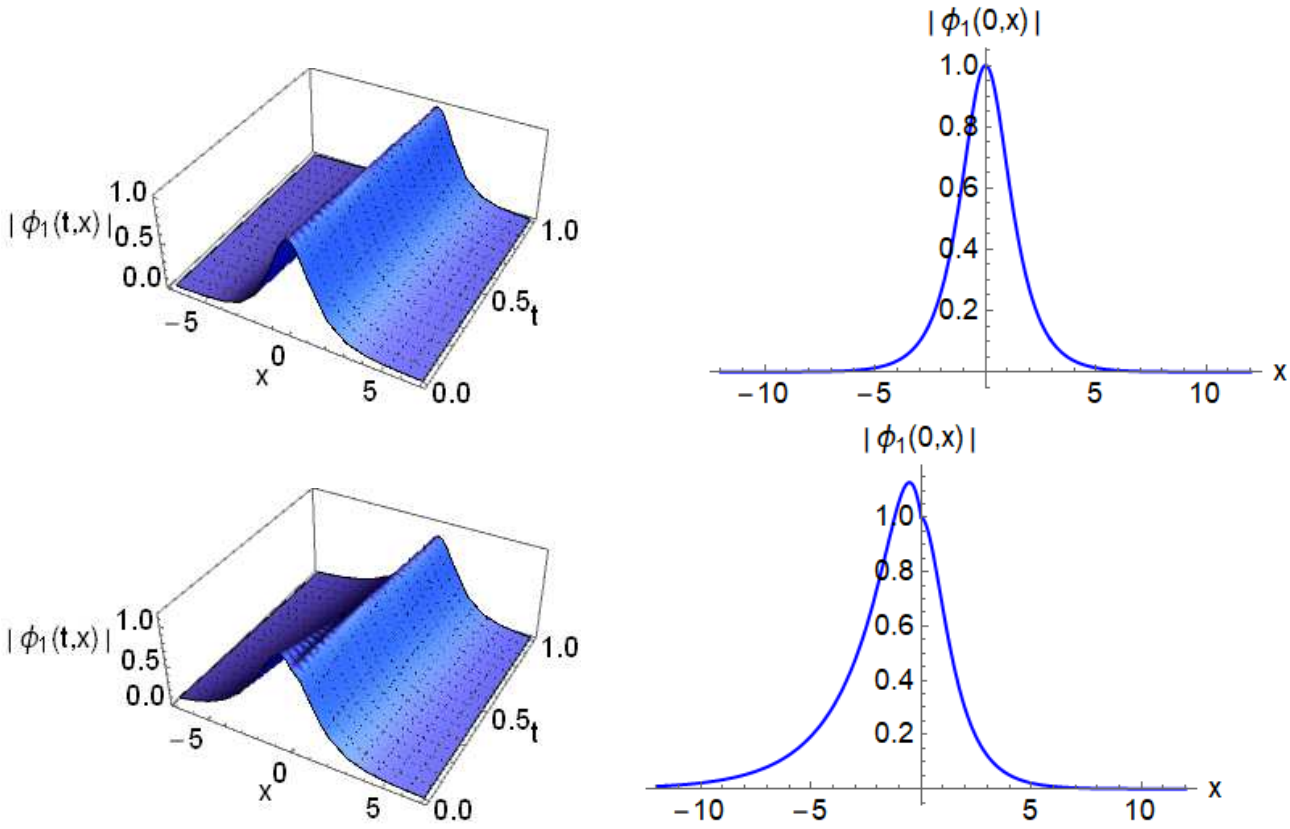

Fig. 1: The bright wave solutions $|\phi_1(t,x)|$ in (15) for the FENSE (1) at $\Pi_1 = \Pi_2 = 1,\ \nu = 1,\ a_1 = 0.008,\ a_2 = 0.005,\ a_3 = 0.025,\ \delta = 1,\ \eta = 1$ such that (a) 3D plot at $\alpha = 1$; (b) 2D plot at $\alpha = 1$; (c) 3D plot at $\alpha = 0.95$; (d) 2D plot at $\alpha = 0.95$.

bright wave. This appears in that the wave in the classical case, $\alpha = 1$, looks symmetrical, which changes when the order of the derivative varies to become fractional, $\alpha = 0.95$.

In Figure 2, we introduce the impact of the fractional derivative on the effective electric field amplitude $E^2 = |\phi_1(t,x)|^2$ where we consider different fractional derivative orders, $\alpha = 0.99,\ 0.95,\ 0.93$ and 0.92. In Figure 2(a), the velocity of the wave ν considered to be 1, while it be $\nu = 1.2$ in Figure 2(b). We notice that both the amplitude and the length of the obtained wave become smaller as the wave velocity increases. Moreover, the crest of the wave shifts to the left as the order of the fractional derivative decreases.

We depicted in Figure 3 the $|\phi_1(t,x)|$, $Re(\phi(t,0)$ and $Im(\phi(t,0))$ against the time t of the bright wave solutions $\phi_1(t,x)$ in (15) for the FENSE (1) at different values for the wave velocity ν and fractional derivative order α.

4.2. Bright wave solution II

We can establish bright wave solutions for the FENSE (1) using another assumption of the solution for the nonlinear ODE (7), which reads:

$$\Phi(\chi) = \frac{\Pi_1}{\sqrt{1+\cosh(\Pi_2\chi)}}, \tag{17}$$

where Π_1 and Π_2 are parameters. We substitute the solution (17) into the ODE (7) and after some simplifications, with aid of Mathematica software packages, we collect the coefficients of the linearly independent terms and set it to be zero, which give us an algebraic system has the following solutions:

$$\Pi_1^{\pm} = \pm\Pi_2\nu\sqrt{\frac{-a_3}{2(3b_1+2b_2)}}, \tag{18}$$

$$\sigma_{1,2} = \frac{a_2}{a_3} \pm \frac{\sqrt{576\nu^2a_2^2 + 48\nu a_3(24 - 24\nu a_1 + B^2\nu^3 a_3)}}{24\nu a_3}, \tag{19}$$

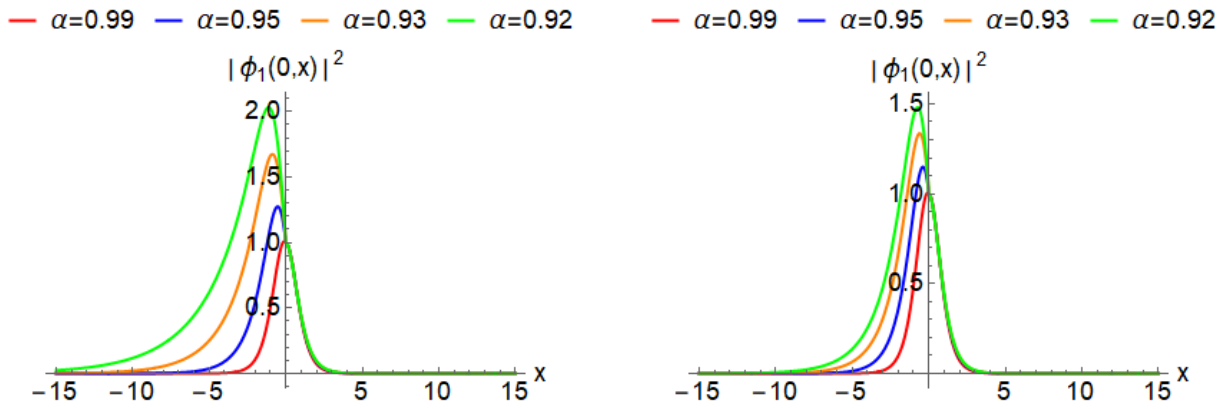

Fig. 2: The effective electric field amplitude $E^2 = |\phi_1(0,x)|^2$ for the FENSE (1) at $\Pi_1 = \Pi_2 = 1,\ a_1 = 0.008,\ a_2 = 0.005,\ a_3 = 0.025,\ \delta = 1,\ \eta = 1$ and at different fractional derivative orders $\alpha = 0.99,\ 0.95,\ 0.93,\ 0.92$ such that (a) $\nu = 1$; (b) $\nu = 1.2$.

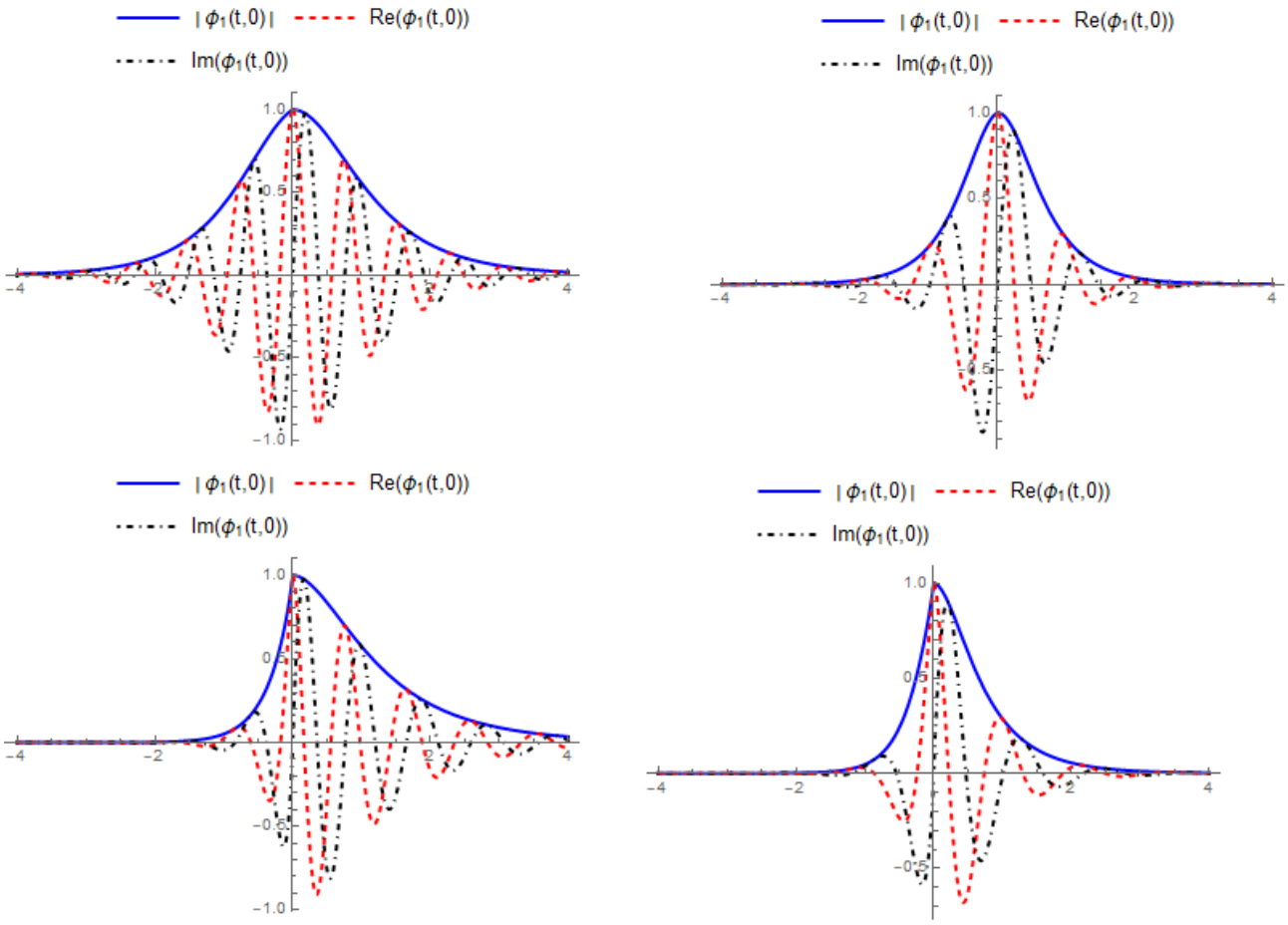

Fig. 3: 2D plots for the $|\phi_1(t,x)|$, $Re(\phi(t,0)$ and $Im(\phi(t,0))$ of the bright wave solutions $\phi_1(t,x)$ in (15) for the FENSE (1) at $\Pi_1 = \Pi_2 = 1,\ \nu = 1,\ a_1 = 0.008,\ a_2 = 0.005,\ a_3 = 0.025,\ \delta = 1,\ \eta = 1$ such that (a) $\alpha = 0.99$ and $\nu = 1.2$; (b) $\alpha = 0.99$ and $\nu = 2$; (c) $\alpha = 0.9$ and $\nu = 1.2$; (d) $\alpha = 0.9$ and $\nu = 2$.

provided that $3b_1+2b_2\neq 0$ and $\nu a_3\neq 0$. Using the obtained results (18-19) into (8) and (9), we obtain the following results for the effective nonlinear coefficient μ and the wave frequency ρ, respectively:

$$\mu_{1,2}=\frac{a_2\left(\nu+3(-1+\nu)b_1+2(-1+\nu)b_2\right)}{\nu a_3}\pm\frac{(\nu-3b_1-2b_2)\sqrt{\nu\left(12\nu a_2^2+a_3\left(24-24\nu a_1+B^2\nu^3a_3\right)\right)}}{2\sqrt{3}\nu^2a_3}, \tag{20}$$

$$\begin{aligned}\rho_{1,2}=&\frac{a_2\left(8a_2^2-3a_3\left(8a_1+B^2(-1+\nu)\nu a_3\right)\right)}{24a_3^2}\\&+\frac{\left(\pm 24\nu a_2^2-a_3\left(24+48\nu a_1+B^2(-9+\nu)\nu^2a_3\right)\right)\sqrt{\nu\left(12\nu a_2^2+a_3\left(24-24\nu a_1+B^2\nu^3a_3\right)\right)}}{144\sqrt{3}\nu^2a_3^2}.\end{aligned} \tag{21}$$

Using (17), we get the following wave profiles:

$$\Phi_{1,2}(\chi)=\frac{\pm\Pi_2\nu\sqrt{\frac{-a_3}{2(3b_1+2b_2)}}}{\sqrt{1+\cosh(\Pi_2\chi)}}. \tag{22}$$

Consequently, with aid of the complex traveling wave transformation (4), we get the following bright wave solutions for the FENSE (1):

$$\phi_{1,2}(t,x)=\frac{\pm\Pi_2\nu\sqrt{\frac{-a_3}{2(3b_1+2b_2)}}}{\sqrt{1+\cosh\left(\Pi_2\left(\frac{\Gamma(\eta+1)}{\alpha}x^\alpha-\nu\frac{\Gamma(\eta+1)}{\alpha}t^\alpha\right)\right)}}\times Exp\left[i\left(\rho_{1,2}\frac{\Gamma(\eta+1)}{\alpha}x^\alpha+\sigma_{1,2}\frac{\Gamma(\eta+1)}{\alpha}t^\alpha+\delta\right)\right], \tag{23}$$

where $\sigma_{1,2}$ and $\rho_{1,2}$ as in (19) and (21), respectively. These results illustrated throughout Figures 4-8. We demonstrate the impact of the self-frequency shift parameter b_2 on the obtained wave profile (22) in Figure 4. We notice that the height of the wave is less as the value of the self-frequency shift parameter b_2 increases, while the wave maintains its shape and symmetry. Figure 4 also shows the effect of parameter b_2 at two different values of the third-order dispersion parameter a_3, Figure 4(a) at $a_3=0.025$ and Figure 4(b) at $a_3=0.1$, as we note that the crest of the wave is larger at the lower value of the third-order dispersion parameter a_3. In Figure 5, we depicted bright wave solutions $|\phi_1(t,x)|$ in (23) for the FENSE (1) in 3D and 2D plots when the derivative order α has consider in classical case $\alpha 1$ and fractional case $\alpha=0.97$. In the classical case $\alpha=1$ the bright wave is symmetric about the $|\phi_1(t,x)|$-axis when the time $t=0$, see Figure 5(b), while the wave symmetry is affected when the fractional derivative $\alpha=0.97$, see Figure 5(d) noting that the effect was on the negative x-axis.

The effective electric field amplitude $E^2=|\phi_1(0,x)|^2$ for the FENSE (1) has illustrated throughout Figures 6 and 7. We Showed the impact of the varity of the fractional derivative order α on the behavior of the obtained electric field amplitude. Figure 6 has depicted at different wave velocity $\nu=2$ and $\nu=3$, while Figure 7 considers various values for the self-frequency shift parameter $b_2=0.1$ and $b_2=1$.

We depicted in Figure 8 the $|\phi_1(0,x)|$, $Re(\phi(t,0)$ and $Im(\phi(t,0))$ against the time t of the bright wave solutions $\phi_1(t,x)$ in (23) for the FENSE (1) at different values for the wave velocity ν and fractional derivative order α.

4.3. Kink wave solution

We will construct kink wave solutions for the FENSE (1) by assuming the nonlinear ODE (7) has a solution in the form:

$$\Phi(\chi)=\Pi_1\tanh(\Pi_2\chi), \tag{24}$$

where Π_1 and Π_2 are constants to be determined. Inserting (24) into the ODE (7), then collect the coefficients of the independent terms in the obtained expression, after some simplifications, to get an algebraic system has the following solutions:

Case 1:

$$\Pi_1^{\pm}=\pm\frac{1}{a_2}\sqrt{\frac{3\left(2a_2^2-\nu a_1^2a_3\right)}{2\nu\left(3b_1+2b_2\right)}},\Pi_2^{\pm}=\pm\frac{1}{\nu^{\frac{3}{2}}a_2}\sqrt{\frac{3\left(2a_2^2-\nu a_1^2a_3\right)}{2a_3}},\ \sigma=\frac{a_1}{a_2}, \tag{25}$$

Case 2:

$$\Pi_1^{\pm}=\pm\Pi_2\nu\sqrt{\frac{a_3}{3b_1+2b_2}},\ \sigma^{\pm}=\pm\sqrt{\frac{2\left(3-\Pi_2^2\nu^3a_3\right)}{3\nu a_3}},a_1=a_2=0,\ \Pi_2\ arbitrary. \tag{26}$$

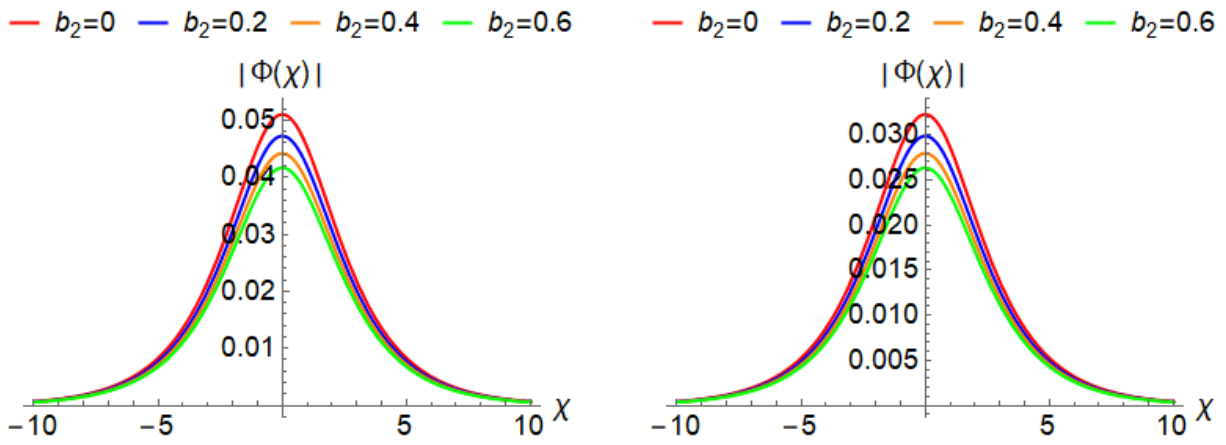

Fig. 4: The wave profile $\Phi(\chi)$ in (22) at $\Pi_2 = 1,\ \nu = 1$ and different values for the self-frequency shift parameter $b_2 = 0,\ 0.2,\ 0.4,\ 0.6$ such that (a) $a_3 = 0.025$; (b) $a_3 = 0.1$.

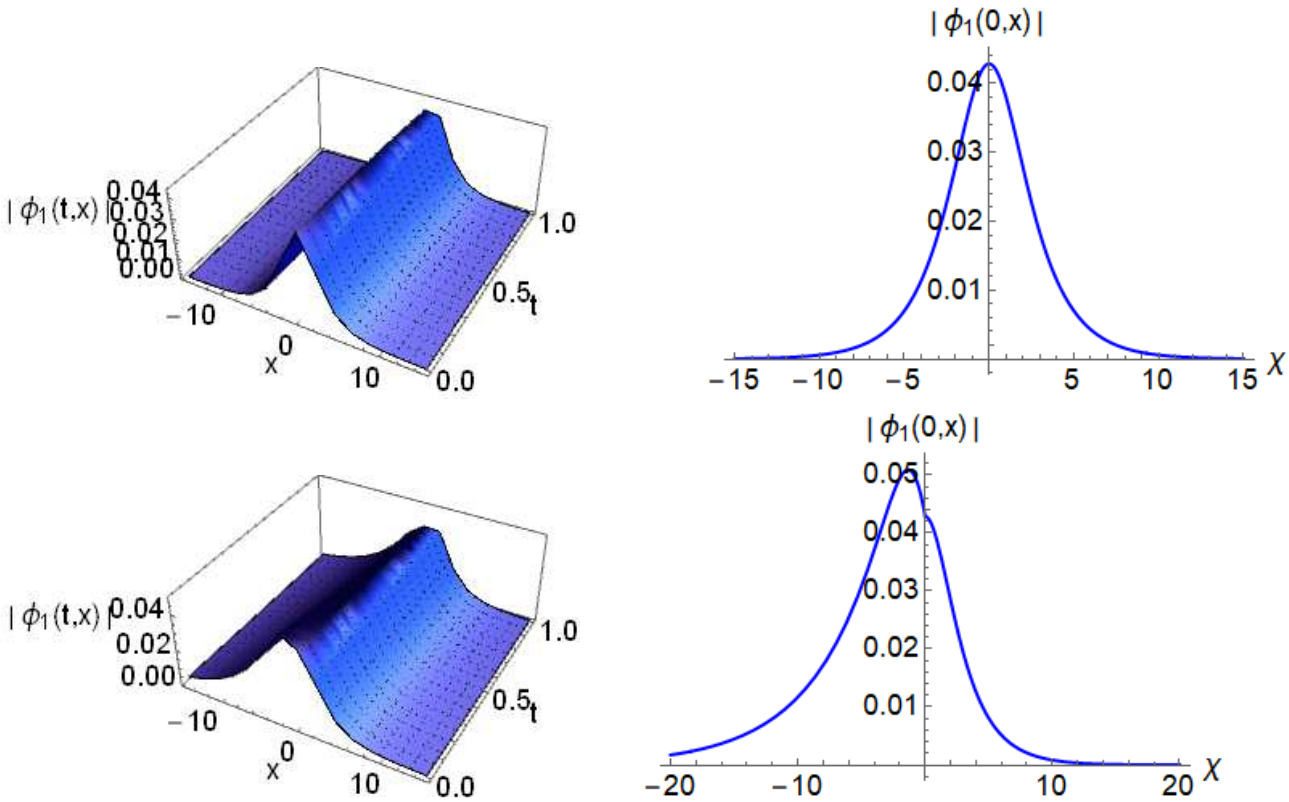

Fig. 5: The bright wave solutions $|\phi_1(t,x)|$ in (23) for the FENSE (1) at $\Pi_2 = 1,\ \nu = 1,\ a_1 = 0.008,\ a_2 = 0.005,\ a_3 = 0.025,\ b_1 = 0.8,\ b_2 = 0.5,\ \delta = 1,\ \eta = 1$ such that (a) 3D plot at $\alpha = 1$; (b) 2D plot at $\alpha = 1$; (c) 3D plot at $\alpha = 0.97$; (d) 2D plot at $\alpha = 0.97$.

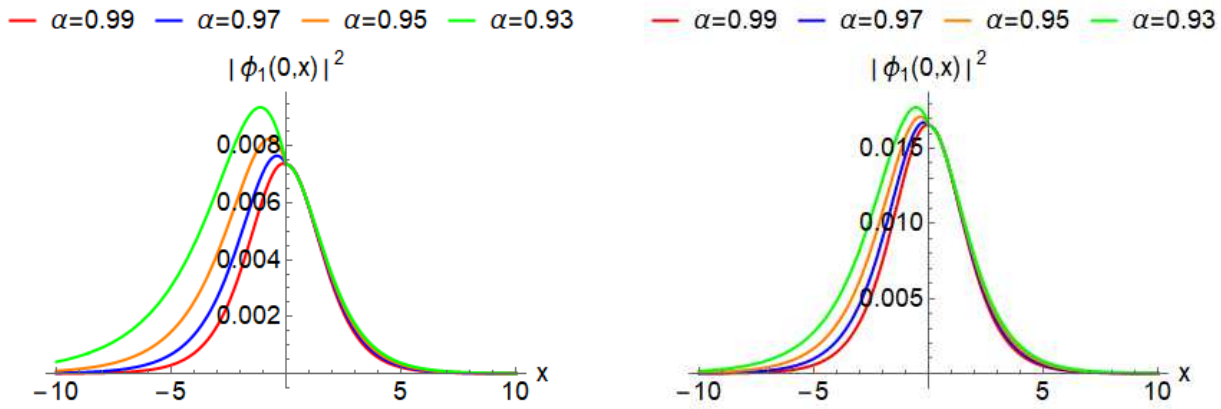

Fig. 6: The effective electric field amplitude $E^2 = |\phi_1(0,x)|^2$ for the FENSE (1) at $\Pi_2 = 1$, $a_1 = 0.008$, $a_2 = 0.005$, $a_3 = 0.025$, $b_1 = 0.8$, $b_2 = 0.5$, $\delta = 1$, $\eta = 1$ and at different fractional derivative orders $\alpha = 0.99,\ 0.97,\ 0.95,\ 0.93$ such that (a) $\nu = 2$; (b) $\nu = 3$.

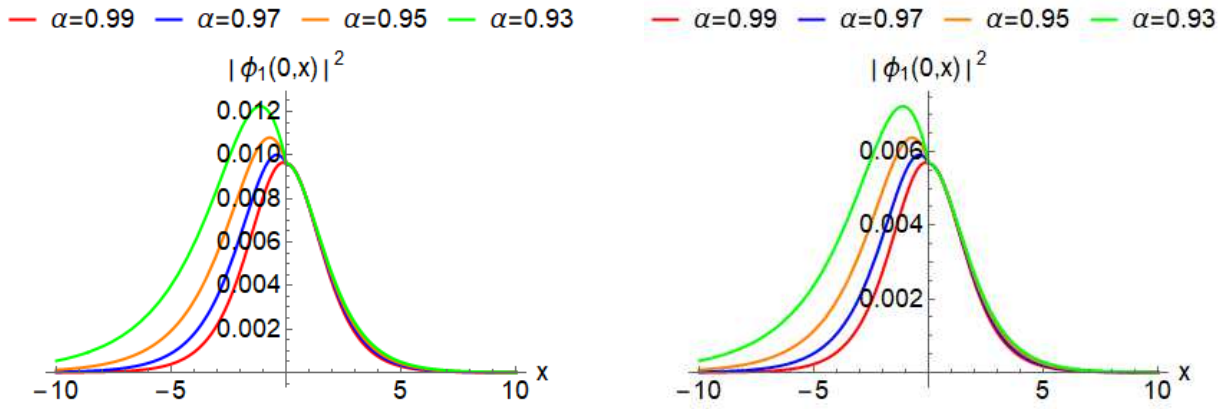

Fig. 7: The effective electric field amplitude $E^2 = |\phi_1(0,x)|^2$ for the FENSE (1) at $\Pi_2 = 1$, $\nu = 2$, $a_1 = 0.008$, $a_2 = 0.005$, $a_3 = 0.025$, $b_1 = 0.8$, $\delta = 1$, $\eta = 1$ and at different fractional derivative orders $\alpha = 0.99,\ 0.97,\ 0.95,\ 0.93$ such that (a) $b_2 = 0.1$; (b) $b_2 = 1$.

provided that $a_3 \neq 0$, $\nu \neq 0$ and $3b_1 + 2b_2 \neq 0$. Depending on these results, the effective nonlinear coefficient μ and the wave frequency ρ can obtained as:

Case 1:

$$\mu = \frac{a_1}{a_2} - \frac{3a_1b_1}{\nu a_2} + \frac{3a_2b_1}{a_3} - \frac{2a_1b_2}{\nu a_2} + \frac{2a_2b_2}{a_3}, \tag{27}$$

$$\rho = -\frac{3a_1}{\nu^2 a_2} - \frac{2a_1^2}{a_2} + \frac{3a_2}{\nu a_3} - \frac{a_1^3 a_3}{6a_2^3} + \frac{3a_1^3 a_3}{2\nu a_2^3}. \tag{28}$$

Case 2:

$$\mu^{\pm} = \pm(\nu - 3b_1 - 2b_2)\sqrt{\frac{2\left(3 - B^2\nu^3 a_3\right)}{3\nu^3 a_3}}, \tag{29}$$

$$\rho^{\pm} = \frac{\pm\left(3 - \Pi_2^2(\nu - 9)\nu^2 a_3\right)}{27}\sqrt{\frac{18 - 6B^2\nu^3 a_3}{\nu^3 a_3}}. \tag{30}$$

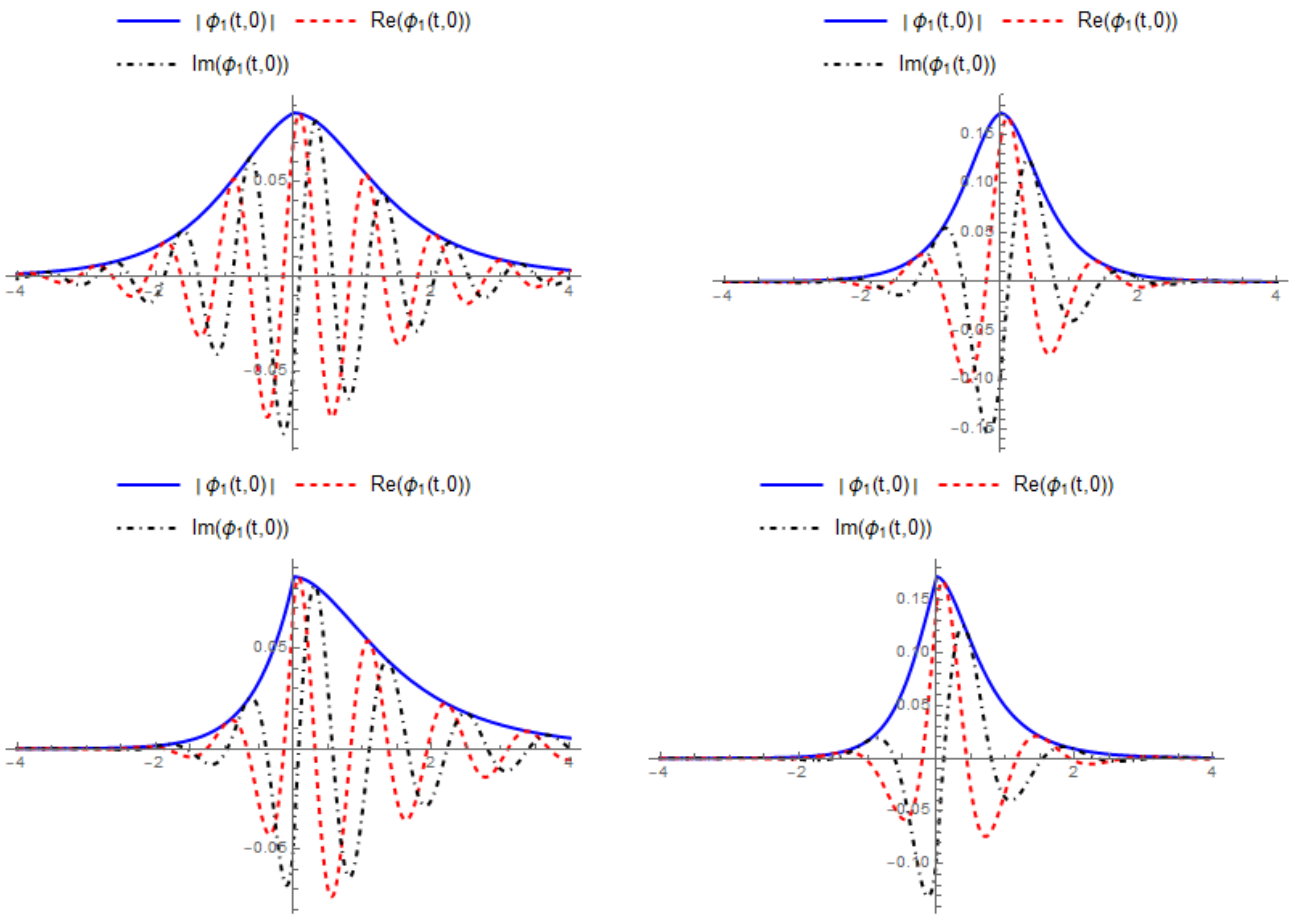

Fig. 8: 2D plots for the $|\phi_1(t,x)|$, $Re(\phi(t,0)$ and $Im(\phi(t,0))$ of the bright wave solutions $\phi_1(t,x)$ in (23) for the FENSE (1) at $\Pi_2 = 1$, $a_1 = 0.008$, $a_2 = 0.005$, $a_3 = 0.025$, $b_1 = 0.8$, $b_2 = 0.5$, $\delta = 1$, $\eta = 1$ such that (a) $\alpha = 0.99$ and $\nu = 2$; (b) $\alpha = 0.99$ and $\nu = 4$; (c) $\alpha = 0.92$ and $\nu = 2$; (d) $\alpha = 0.92$ and $\nu = 4$.

The wave profile $\Phi(\chi)$ can be given as:

$$\Phi_1^{\pm}(\chi) = \pm\frac{1}{a_2}\sqrt{\frac{3\left(2a_2^2 - \nu a_1^2 a_3\right)}{2\nu\left(3b_1+2b_2\right)}}\tanh\left(\left(\pm\frac{1}{\nu^{\frac{3}{2}}a_2}\sqrt{\frac{3\left(2a_2^2-\nu a_1^2a_3\right)}{2a_3}}\right)\chi\right), \tag{31}$$

$$\Phi_2^{\pm}(\chi) = \pm\Pi_2\nu\sqrt{\frac{a_3}{3b_1+2b_2}}\tanh\left(\Pi_2\chi\right), \tag{32}$$

where $\Phi_1^{\pm}(\chi)$ have obtained according to the Case 1, while $\Phi_1^{\pm}(\chi)$ constructed using Case 2. Consequently, with aid of the complex traveling wave transformation (9), we get the following kink wave solutions for the FENSE (1):

$$\begin{aligned}\phi_1(t,x) = {} & \frac{1}{a_2}\sqrt{\frac{3\left(2a_2^2-\nu a_1^2a_3\right)}{2\nu\left(3b_1+2b_2\right)}}\times\tanh\left(\left(\frac{1}{\nu^{\frac{3}{2}}a_2}\sqrt{\frac{3\left(2a_2^2-\nu a_1^2a_3\right)}{2a_3}}\right)\left(\frac{\Gamma(\eta+1)}{\alpha}x^{\alpha} - \nu\frac{\Gamma(\eta+1)}{\alpha}t^{\alpha}\right)\right)\\ & \times Exp\left[i\left(\left(-\frac{3a_1}{\nu^2a_2}-\frac{2a_1^2}{a_2}+\frac{3a_2}{\nu a_3}-\frac{a_1^3a_3}{6a_2^3}+\frac{3a_1^3a_3}{2\nu a_2^3}\right)\frac{\Gamma(\eta+1)}{\alpha}x^{\alpha}+\left(\frac{a_1}{a_2}\right)\frac{\Gamma(\eta+1)}{\alpha}t^{\alpha}+\delta\right)\right],\end{aligned} \tag{33}$$

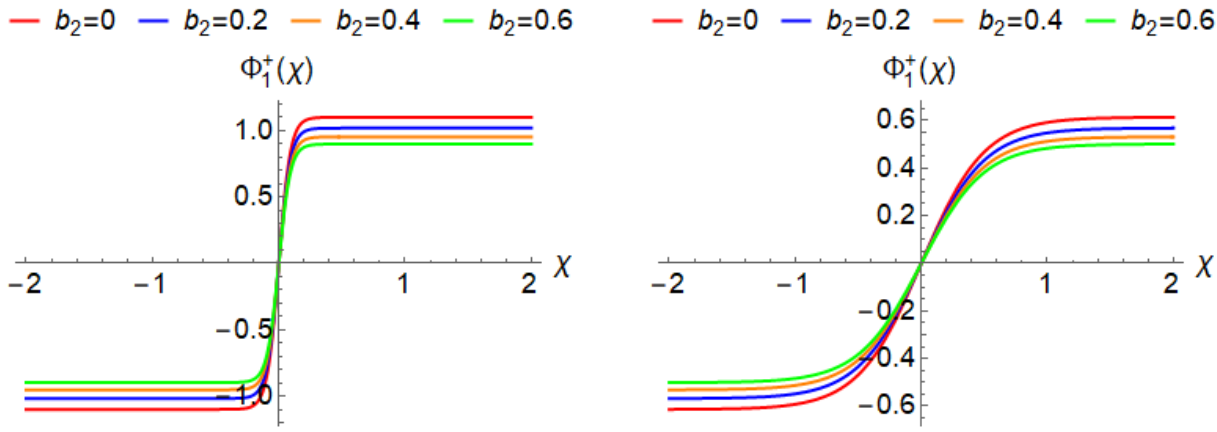

Fig. 9: The wave profile $\Phi_1^+(\chi)$ in (31) at $a_1 = 0.008,\ a_2 = 0.005,\ a_3 = 0.025,\ b_1 = 0.8$ and different values for the self-frequency shift parameter $b_2 = 0,\ 0.2,\ 0.4,\ 0.6$ such that (a) $v = 1$; (b) $v = 3$.

$$\phi_2(t,x) = \frac{-1}{a_2}\sqrt{\frac{3\left(2a_2^2 - va_1^2a_3\right)}{2v\left(3b_1+2b_2\right)}} \times \tanh\left(\left(\frac{-1}{v^{\frac{3}{2}}a_2}\sqrt{\frac{3\left(2a_2^2 - va_1^2a_3\right)}{2a_3}}\right)\left(\frac{\Gamma(\eta+1)}{\alpha}x^{\alpha} - v\frac{\Gamma(\eta+1)}{\alpha}t^{\alpha}\right)\right)$$
$$\times Exp\left[i\left(\left(-\frac{3a_1}{v^2a_2} - \frac{2a_1^2}{a_2} + \frac{3a_2}{va_3} - \frac{a_1^3a_3}{6a_2^3} + \frac{3a_1^3a_3}{2va_2^3}\right)\frac{\Gamma(\eta+1)}{\alpha}x^{\alpha} + \left(\frac{a_1}{a_2}\right)\frac{\Gamma(\eta+1)}{\alpha}t^{\alpha} + \delta\right)\right], \tag{34}$$

$$\phi_3(t,x) = -\Pi_2 v\sqrt{\frac{a_3}{3b_1+2b_2}} \times \tanh\left(\Pi_2\left(\frac{\Gamma(\eta+1)}{\alpha}x^{\alpha} - v\frac{\Gamma(\eta+1)}{\alpha}t^{\alpha}\right)\right)$$
$$\times Exp\left[i\left(\rho^{+}\frac{\Gamma(\eta+1)}{\alpha}x^{\alpha} + \left(\sqrt{\frac{2\left(3-\Pi_2^2v^3a_3\right)}{3va_3}}\right)\frac{\Gamma(\eta+1)}{\alpha}t^{\alpha} + \delta\right)\right], \tag{35}$$

$$\phi_4(t,x) = \Pi_2 v\sqrt{\frac{a_3}{3b_1+2b_2}} \times \tanh\left(\Pi_2\left(\frac{\Gamma(\eta+1)}{\alpha}x^{\alpha} - v\frac{\Gamma(\eta+1)}{\alpha}t^{\alpha}\right)\right)$$
$$\times Exp\left[i\left(\rho^{-}\frac{\Gamma(\eta+1)}{\alpha}x^{\alpha} + \left(-\sqrt{\frac{2\left(3-\Pi_2^2v^3a_3\right)}{3va_3}}\right)\frac{\Gamma(\eta+1)}{\alpha}t^{\alpha} + \delta\right)\right]. \tag{36}$$

We show the obtained results in Figures 9-13. In Figure 9 we present the kink wave profile $\Phi_1^+(\chi)$ in (31) at selected parameters, while the kink wave profile $\Phi_2^+(\chi)$ in (32) has depicted in Figure 10.

Figure 11 shows the effective electric field amplitude $E^2 = |\phi_1(1,x)|^2$ for the FENSE (1) at different orders for the fractional derivative α such that the wave velocity has considered at $v = 0.2$ and $v = 0.1$. The effective electric field amplitude $E^2 = |\phi_3(3,x)|^2$ for the FENSE (1) presented in Figure 12.

It is clear from Figures 11 and 12 that the change in the order of the fractional derivative α changes the behavior of the inferred kink wave. Moreover, this change in behavior is also affected by the velocity of the wave v by comparing Figures (a) and (b) in each of 11 and 12.

Figures 13 and 14 presented the real and imaginary parts of the kink wave solutions $\phi_1(t,x)$ and $\phi_3(t,x)$, respectively.

5 Conclusion

The fractional extended nonlinear Schrödinger equation has been examined in this study by considering the truncated M-fractional derivative meaning. We have reduced the governing model to a nonlinear ordinary differential equation by

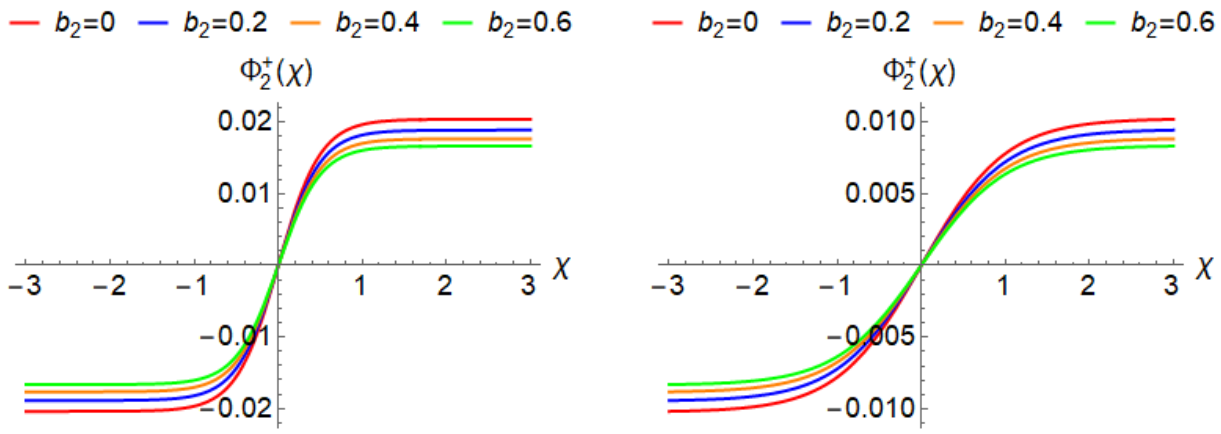

Fig. 10: The wave profile $\Phi_2^+(\chi)$ in (32) at $\nu = 0.1,\ a_3 = 0.025,\ b_1 = 0.8$ and different values for the self-frequency shift parameter $b_2 = 0,\ 0.2,\ 0.4,\ 0.6$ such that (a) $\Pi_2 = 2$; (b) $\Pi_2 = 1.5$.

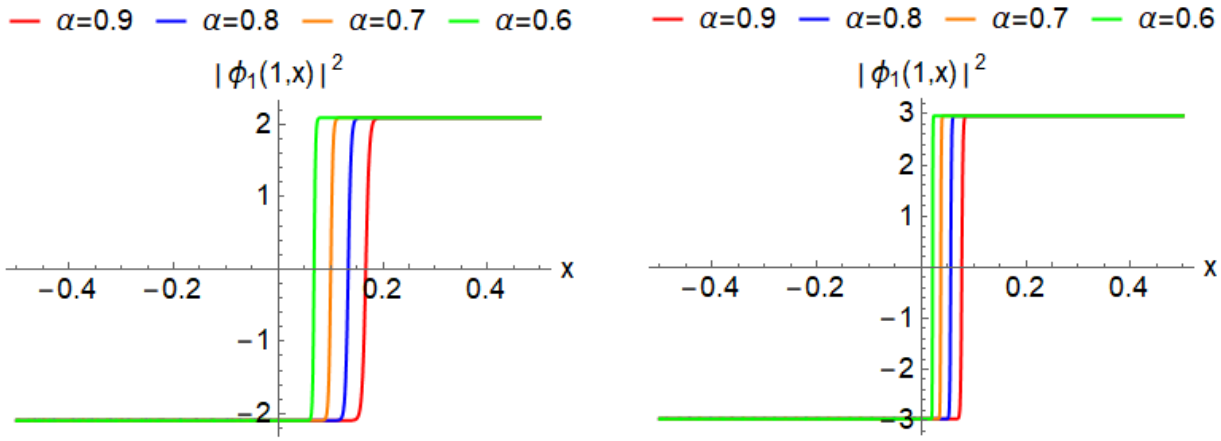

Fig. 11: The effective electric field amplitude $E^2 = |\phi_1(1,x)|^2$ for the FENSE (1) at $a_1 = 0.008,\ a_2 = 0.005,\ a_3 = 0.025,\ b_1 = 0.8,\ b_2 = 0.5, \delta = 1,\ \eta = 1$ and at different fractional derivative orders $\alpha = 0.9,\ 0.8,\ 0.7,\ 0.6$ such that (a) $\nu = 0.2$; (b) $\nu = 0.1$.

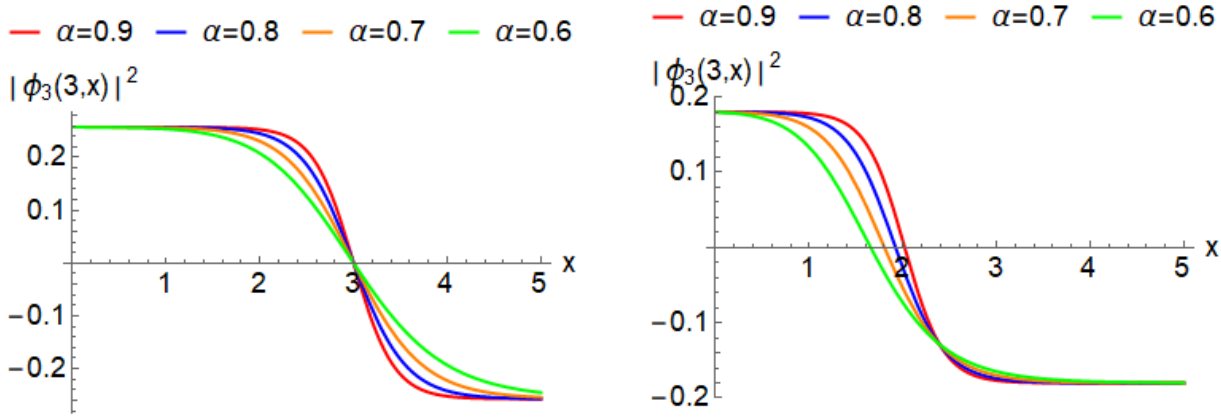

Fig. 12: The effective electric field amplitude $E^2 = |\phi_1(3,x)|^2$ for the FENSE (1) at $\Pi_2 = 3,\ a_3 = 0.025,\ b_1 = 0.8,\ b_2 = 0.5, \delta = 1,\ \eta = 1$ and at different fractional derivative orders $\alpha = 0.9,\ 0.8,\ 0.7,\ 0.6$ such that (a) $\nu = 0.2$; (b) $\nu = 0.7$.

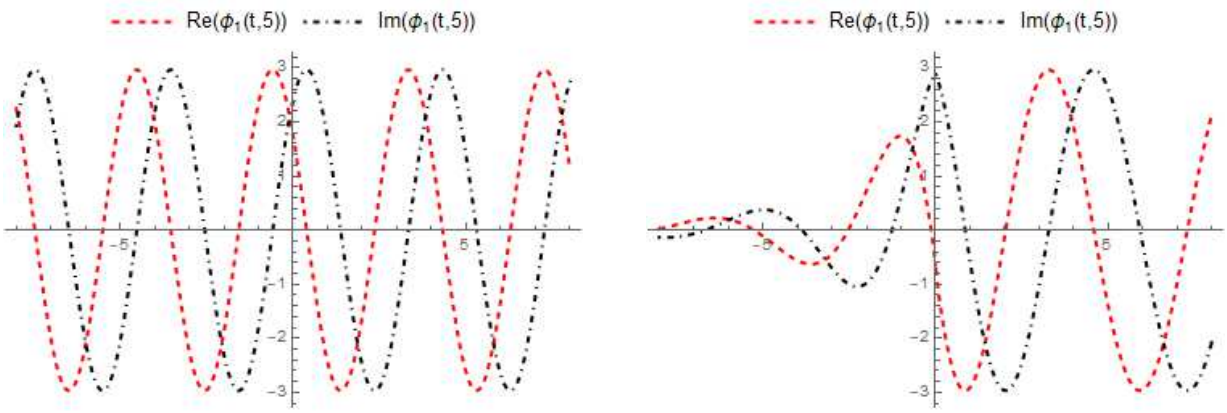

Fig. 13: 2D plots for the $Re(\phi_1(t,5)$ and $Im(\phi_1(t,5))$ of the kink wave solutions $\phi_1(t,x)$ for the FENSE (1) at $\nu = 0.1,\ a_1 = 0.008,\ a_2 = 0.005,\ a_3 = 0.025,\ b_1 = 0.8,\ b_2 = 0.5, \delta = 1,\ \eta = 1$ such that (a) $\alpha = 1$; (b) $\alpha = 0.9$.

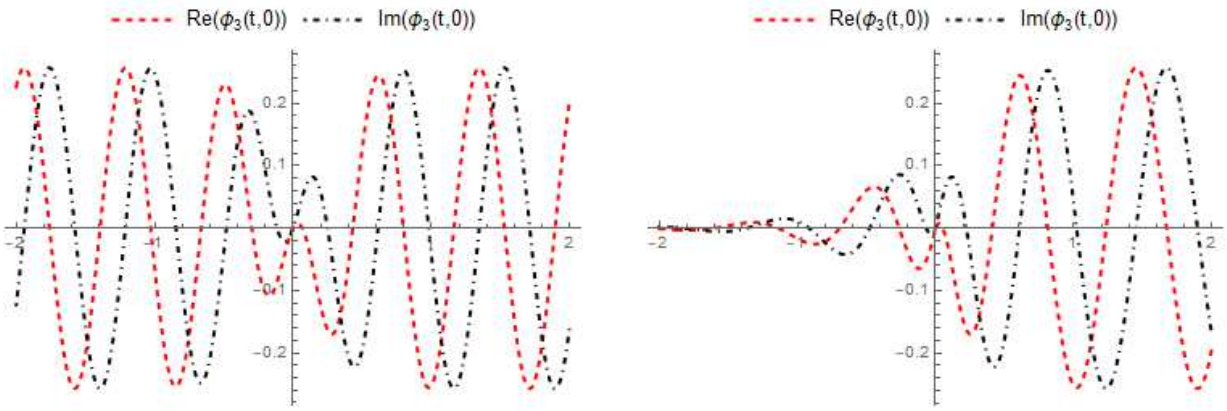

Fig. 14: 2D plots for the $Re(\phi_3(t,0)$ and $Im(\phi_3(t,0))$ of the kink wave solutions $\phi_3(t,x)$ for the FENSE (1) at $\nu = 1,\ \Pi_2 = 3,\ a_3 = 0.025,\ b_1 = 0.8,\ b_2 = 0.5, \delta = 1,\ \eta = 1$ such that (a) $\alpha = 1$; (b) $\alpha = 0.9$.

applying a complex traveling wave transformation. Traveling wave solutions for the model, specifically bright and kink wave solutions, have been obtained using the Ansatz approach. The obtained solutions satisfy certain parameter requirements. We have represented the established traveling wave solutions using 3D and 2D plots at particular parameter values to provide insight into their physical nature. This visualization helps in better comprehending the behavior and traits of the solutions. Additionally, we have investigated how the characteristics of the resulting solutions are impacted by the fractional derivative. Overall, our results demonstrate the existence of bright and kink wave solutions to the fractional extended nonlinear Schrödinger equation with certain properties. Exploring these solutions offers important new perspectives on the dynamics of nonlinear systems. Our research advances the understanding of fractional derivatives and their effects on wave propagation in nonlinear media. Further exploration of different types of solutions and the behavior of the fractional extended nonlinear Schrödinger equation in various settings is possible.

References

[1] Y. Kodama and A. Hasegawa, Nonlinear pulse propagation in a monomode dielectric guide, *IEEE J. Quant. Electr.* **23**(5), 510-524 (1987).
[2] M. Jain and N. Tzoar, Nonlinear pulse propagation in optical fibers, *Opt. Lett.* **3**(5), 202-204 (1978).
[3] J. P. Gordon, Theory of the soliton self-frequency shift, *Opt. Lett.* **11**(10), 662-664 (1986).
[4] M. Al-Smadi, O. A. Arqub and S. Momani, Numerical computations of coupled fractional resonant Schrödinger equations arising in quantum mechanics under conformable fractional derivative sense, *Phys. Scripta* **95**(7), 075218 (2020).

[5] M. Alabedalhadi, M. Al-Smadi, S. Al-Omari, D. Baleanu and S. Momani, S. Structure of optical soliton solution for nonliear resonant space-time Schrödinger equation in conformable sense with full nonlinearity term, *Phys. Scripta* **95**(10), 105215 (2020).
[6] M. Shqair, M. Al-Smadi, S. Momani and E. El-Zahar, Adaptation of conformable residual power series scheme in solving nonlinear fractional quantum mechanics problems, *Appl. Sci.* **10**(3), 890 (2020.
[7] S. Momani, N. Djeddi, M. Al-Smadiand and S. Al-Omari, Numerical investigation for Caputo-Fabrizio fractional Riccati and Bernoulli equations using iterative reproducing kernel method, *Appl. Numer. Math.* **170**, 418-434 (2021).
[8] M. Alabedalhadi, M. Shqair, S. Al-Omari and M. Al-Smadi, Traveling wave solutions for complex space-time fractional Kundu-Eckhaus equation, *Mathematics*, **11**(2), 404 (2023).
[9] J. Y. Qiu, A. Grimsmo, K. Peng, B. Kannan, B. Lienhard, Y. Sung, ... and W. D. Oliver, Broadband squeezed microwaves and amplification with a Josephson travelling-wave parametric amplifier, *Nature Phys.* 1-8 (2023).
[10] A. Burqan, A. El-Ajou, R. Saadeh, M. Al-Smadi, A new efficient technique using Laplace transforms and smooth expansions to construct a series solution to the time-fractional Navier-Stokes equations, *Alexandria Eng. J.* **61**(2), 1069-1077 (2022).
[11] M. A. Al-Smadi, O. Arqub and S. Hadid, Approximate solutions of nonlinear fractional Kundu-Eckhaus and coupled fractional massive Thirring equations emerging in quantum field theory using conformable residual power series method, *Phys. Scripta* **95**(10), 105205 (2020).
[12] A. El-Ajou, M. Al-Smadi, M. O. Moa'ath, S. Momani and S. Hadid, Smooth expansion to solve high-order linear conformable fractional PDEs via the residual power series method: Applications to physical and engineering equations, *Ain Shams Eng. J.* **11**(4), 1243-1254 (2020).
[13] M. Shqair, M. Alabedalhadi, S. Al-Omari and M. Al-Smadi, Abundant exact travelling wave solutions for a fractional massive Thirring model using extended Jacobi elliptic function method, *Frac. Fract.* **6**(5), 252 (2022).
[14] M. Esposito, A. Ranadive, L. Planat and N. Roch, Perspective on traveling wave microwave parametric amplifiers, *Appl. Phys. Lett.* **119**(12) (2021.
[15] Y. Yuan, M. Haider, J. A. Russer, P. Russer and C. Jirauschek, Circuit quantum electrodynamic model of dissipative-dispersive Josephson traveling-wave parametric amplifiers, *Phys. Rev. A* **107**(2), 022612 (2023).
[16] H. Rezazadeh, F. Batool, M. Inc, L. Akinyemi and M. S. Hashemi, Exact traveling wave solutions of generalized fractional Tzitz eica-type nonlinear evolution equations in nonlinear optics, *Opt. Quant. Elect.* **55**(6), 485 (2023).
[17] C. Bartrame et al., Dark matter axion search using a Josephson traveling wave parametric amplifier, *Rev. Sci. Instr.* **94**(4) (2023).
[18] M. M. Khater, S. H. Alfalqi, J. F. Alzaidi and R.A. Attia, Novel soliton wave solutions of a special model of the nonlinear Schrödinger equations with mixed derivatives, *Res. Phys.* **47**, 106367 (2023).
[19] Z. Li and Z. Liu, Optical solitons and single traveling wave solutions for the Triki–Biswas equation describing monomode optical fibers, *Optik* **258**, 168835 (2022).
[20] W. H. Zhu and J. G. Liu, Bright and dark solitons for the fifth-order nonlinear Schrödinger equation with variable coefficients, *Optik*, **276**, 170618 (2023).
[21] I. Hamid and S. Kumar, Symbolic computation and Novel solitons, traveling waves and soliton-like solutions for the highly nonlinear (2+ 1)-dimensional Schrödinger equation in the anomalous dispersion regime via newly proposed modified approach, *Opt. Quant. Electr.* **55**(9), 755 (2023).
[22] C. Li, D. Qian and Y. Chen, On Riemann-Liouville and Caputo derivatives, *Disc. Dynam. Nat. Soc.* **15**(1) DOI:10.1155/2011/562494 (2011).
[23] Almeida, R. (2017). A Caputo fractional derivative of a function with respect to another function,*Commun. Nonlin. Sci. Numer. Simul.* **44**, 460-481 (2017).
[24] Y. Y. Gambo, F. Jarad, D. Baleanu and T. Abdeljawad, On Caputo modification of the Hadamard fractional derivatives, *Adv. Differ. Equ.* **2014**(1), 1-12 (2014).
[25] Y. Adjabi, F. Jarad, D. Baleanu and T. Abdeljawad, On Cauchy problems with Caputo Hadamard fractional derivative, *J. Comput. Anal. Appl.* **21**(4), (2016)
[26] Q. Yang, F. Liu and I. Turner, Numerical methods for fractional partial differential equations with Riesz space fractional derivatives, *Appl. Math. Model.* **34**(1), 200-218 (2010).
[27] D. Zhao and M. Luo, General conformable fractional derivative and its physical interpretation, *Calcolo* **54**, 903-917 (2017).
[28] B. Acay, E. Bas and T. Abdeljawad, Non-local fractional calculus from different viewpoint generated by truncated M-derivative, *J. Comput. Appl. Math.* **366**, 112410 (2020).
[29] Z. Zheng, W. Zhao and H. Dai, A new definition of fractional derivative, *Int. J. Nonlin. Mech.* **108**, 1-6 (2019).
[30] M. D. Ortigueira and J. A. Machado, What is a fractional derivative? *J. Comput. Phys.* **293**, 4-13 (2015).
[31] U. N. Katugampola, Correction to "What is a fractional derivative?" by Ortigueira and Machado [Journal of Computational Physics, volume 293, 15 July 2015, pages 4–13. Special issue on Fractional PDEs], *J. Comput. Phys.* **321**, 1255-1257 (2016).
[32] J. V. D. C. Sousa and E. C. de Oliveira, A new truncated $ M $-fractional derivative type unifying some fractional derivative types with classical properties, arXiv preprint arXiv:1704.08187 (2017).
[33] G. A. Dorrego and R. A. Cerutti, The k-Mittag-Leffler function, *Int. J. Contemp. Math. Sci.* **7**(15), 705-716 (2012).
[34] M. Al-Smadi, O. A. Arqub and D. Zeidan, Fuzzy fractional differential equations under the Mittag-Leffler kernel differential operator of the ABC approach: theorems and applications, *Chaos Solit. Fract.* **146**, 110891 (2021).
[35] A. El-Ajou, O. A. Arqub and M. Al-Smadi, A general form of the generalized Taylor's formula with some applications, *Appl. Math. Comput.* **256**, 851-859 (2015).

[36] S.Qureshi, Monotonically decreasing behavior of measles epidemic well captured by Atangana–Baleanu–Caputo fractional operator under real measles data of Pakistan, *Chaos Solit. Fract.*, **131**, 109478 (2020).